Journal of Biomechanics 199 (2026) 113219

Contents lists available at ScienceDirect

Journal of Biomechanics

journal homepage: www.elsevier.com/locate/jbiomech

Average rotation matrices for converting scapula- and glenoid-based coordinate systems to ISB recommendations

Florent Moissenet [a,b,*], Benjamin Michaud [c,d], Pierre Puchaud [e], Nicola Hagemeister [f,g], Mickaël Begon [c,d], Nicolas Holzer [b,h]

[a] Kinesiology Laboratory, Geneva University Hospitals and University of Geneva, Geneva, Switzerland
[b] Biomechanics and Translational Research in Surgery, Department of Surgery, University of Geneva, Geneva, Switzerland
[c] Laboratoire de Simulation et Modélisation du Mouvement, École de Kinésiologie et des Sciences de l'Activité Physique, Faculté de Médecine, Université de Montréal, Montréal, Canada
[d] Centre de recherche Azrieli du CHU Sainte-Justine, Montréal, Canada
[e] Inria center of the University of Bordeaux, 33400 Talence, France
[f] Ecole de Technologie Supérieure, Montréal, Canada
[g] Laboratoire de recherche en imagerie et orthopédie, Centre de recherche du Centre hospitalier de l'Université de Montréal, Montréal, Canada
[h] Orthopedic Surgery and Musculoskeletal Trauma Care Division, Department of Surgery, Geneva University Hospitals, Geneva, Switzerland

ARTICLE INFO

Keywords:
Scapula
Local coordinate system
Rigid body transformation
Statistical shape model
Shoulder

ABSTRACT

Defining bone-embedded local coordinate systems (LCSs) is fundamental in shoulder biomechanics, yet multiple scapular LCSs exist, hindering data comparison. Although the International Society of Biomechanics (ISB) has published recommendations, alternative definitions based on distinct anatomical landmarks remain often used. To address these inconsistencies, average rotation matrices were recently proposed to convert between the three most common scapular LCSs, thereby facilitating comparison, merging, and interoperability between datasets. Building upon this, we have extended the approach to 11 scapular LCSs reported in the literature, including scapula- and glenoid-based systems. Using statistical shape models derived from 80 participants (asymptomatic and pathological shoulders), 1000 scapulae were generated to quantify geometric transformations between LCSs. Average rotation matrices were computed for each alternative system relative to the ISB-recommended LCS, and accuracy was assessed using helical angles. The application of the average rotation matrices substantially reduced the maximal discrepancies between LCSs, from 21.9° to 5.2°. Scapula-based systems exhibited lower discrepancies than glenoid-based ones, reflecting greater morphological variability in the glenoid region. Comparisons with previously published matrices showed minimal differences (<3°), supporting the robustness of the approach across various datasets and population. These findings confirm that average rotation matrices provide a reliable means of harmonising scapular kinematic data across studies, even if experimenters initially chose a different LCS. This work offers a simple framework, for bridging existing scapular kinematic datasets and promoting interoperability datasets in shoulder biomechanics research.

1. Introduction

One key aspect when analysing shoulder kinematics lies in the definition of bone-embedded local coordinate systems (LCSs), which strongly influences the way results can be compared and interpreted. Although the International Society of Biomechanics (ISB) has published recommendations to harmonise these definitions (Wu et al., 2005), notable discrepancies persist in how LCSs are constructed across studies (Kolz et al., 2020; Lawrence et al., 2022; Moissenet et al., 2025b). Such inconsistency limits the comparability of results, restricts data interoperability, and challenges clinical translation. While redefining LCSs directly from imaging or surface models would, in principle, be feasible to eliminate discrepancies between definitions, such data are rarely available in practice. There is therefore a need for post-processing capable of evaluating and compensating for discrepancies between existing LCSs. Hence, rotational and translational offsets between coordinate systems can be minimised, enabling meaningful comparison of kinematic measurements even when different or initially undefined LCSs

* Corresponding author at: Laboratoire de Cinésiologie, HUG, 4 rue Gabrielle-Perret-Gentil Genève 14, CH-1211, Switzerland.
E-mail address: florent.moissenet@unige.ch (F. Moissenet).

https://doi.org/10.1016/j.jbiomech.2026.113219
Accepted 13 February 2026
Available online 17 February 2026

are used.

Focusing on the scapula, a recent review (Spartacus project) (Moissenet et al., 2025b) highlighted that this bone presents 10 alternative LCS definitions relative to the ISB recommendations, mainly due to variations in measurement methods, such as skin marker-based motion capture (e.g., marker-based motion capture) versus imaging-based analysis (e.g., single or biplane fluoroscopy). This has led to two primary categories of LCSs: scapula- and glenoid-based LCSs. However, the diversity of definitions introduces ambiguity when comparing or aggregating kinematic data, as demonstrated by Lawrence et al. (2022), who showed that the choice of LCS substantially influences motion interpretation, despite all definitions are anatomically reasonable.

To address these inconsistencies, (Kolz et al., 2020) proposed a post-process using average rotation matrices to estimate rigid transformations between three common scapula LCSs, with origins at the glenoid centre, posterolateral acromion (ISB recommendation), and acromioclavicular joint. They showed that the scapulothoracic angular kinematics could be reliably converted between these LCSs, with rotational discrepancies not exceeding 4°. This approach builds upon established methodologies for comparing anatomical frames, such as those used for muscle insertion sites (Xu et al., 2012), inertial parameter alignment (Dumas et al., 2007), or coordination frame comparisons in other bones like the humerus (Sulkar et al., 2021). However, the average rotation matrices computed by Kolz et al. (2020) were based on 51 cadaver scapulae and the analysis was limited to only three LCSs. In contrast, the Spartacus project highlighted the existence of 11 distinct scapular LCSs, though comparisons between these systems have yet to be systematically explored.

Our study aims to extend the work of Kolz et al. (2020) by computing the average rotation matrices for these 11 LCSs. This will enable comparative analyses across the existing literature, thereby facilitating interoperability between studies that rely on different LCS definitions. In this context, our aim is not to standardise the choice of LCS, but to provide tools to bridge between them, enabling data interoperability. By quantifying the geometric relationships between a broad set of LCSs, both scapula- and glenoid-based, our study contributes a practical framework to facilitate robust cross-study comparisons in shoulder kinematics research. We expected the proposed approach to remain valid across all LCS definitions, with rotational discrepancies remaining within a similar range to those previously reported by Kolz et al. ($\leq 5°$). We also anticipated that glenoid-based LCSs might yield slightly poorer results due to greater variability in the orientation and morphology of the glenoid relative to the rest of the scapula (Casier et al., 2018; Tokita et al., 2025). Finally, by applying our method to a larger and independent dataset than that used by Kolz et al. (2020), we sought to assess how closely the average rotation matrices obtained here align with theirs. Ultimately, this supports the wider goals of transparency, reproducibility, and data integration in shoulder biomechanics.

2. Methods

2.1. Dataset

The dataset was collected in a previous project (Bascan, 2018; Hagemeister et al., 2014; Yamani, 2022; Zhang, 2016) and includes 80 participants from two distinct populations: an asymptomatic group without shoulder pain or dysfunction (13 women and 15 men; mean age: 56 ± 7 years), and a pathological group diagnosed with full-thickness supraspinatus tendon tears, associated with mild to moderate muscle atrophy (Thomazeau grades 1–2) (Thomazeau et al., 1996), and mainly grade-2 fatty infiltration (Goutallier et al., 1994) of the supraspinatus and infraspinatus muscles (20 women and 32 men; mean age: 56 ± 7 years). Data collection was conducted under ethical approval from the Centre Hospitalier de l'Université de Montréal (CHUM, protocol 09.261), with all participants providing written informed consent.

Biplanar radiographs were acquired using the EOS system (ATEC Spine, USA) with participants standing, arms relaxed, and positioned at approximately 40° of axial rotation relative to the anterior-posterior view. The images and a generic scapula surface model were processed in the IdefX image-processing software (IBHGC, Arts et Métiers Sciences et Technologies, France; LIO, ÉTS, Québec, Canada) for 2D-3D registration. Briefly, the registration method followed the approach of Zhang (2016), using the generic scapula model developed by Ohl et al. (2012) composed of 20,148 triangular faces and 10,078 vertices. Model alignment was refined using a moving least squares deformation algorithm (Cresson et al., 2008) to fit the radiological contours. The algorithm estimates a locally optimal affine transformation at each surface point, weighted by its distance to nearby control handles, thus maintaining geometric fidelity while allowing smooth, non-rigid deformations, particularly around the glenoid, coracoid process, scapular spine, and medial border.

In line with previous studies (Churchill et al., 2001; İncesoy et al., 2021; Moor et al., 2013; Satir et al., 2024; Smith et al., 2022; Zhou et al., 2022), a set of six morphological parameters were extracted from each participant's model (Table 1) to characterise scapular shape. To ensure that the dataset captured populations with distinct scapular morphologies and thus provided a broader morphological basis for testing the robustness and generalisability of the average rotation matrix approach, series of t-tests were performed to compare the morphological parameters between the two groups.

2.2. Statistical shape models

A statistical shape model (SSM) was generated from the dataset for each of the two groups following the method described by Yamani (2022). First, the left scapulae were mirrored to match the orientation of the right scapulae, aligning all models to a unified reference. Second, the scapula models were aligned within a common coordinate system using generalized Procrustes analysis (Umeyama, 1991). This procedure removes differences in translation, rotation, and scale, preserving only anatomical shape variations. Third, a principal component analysis (PCA) was conducted separately on the asymptomatic and pathological SSMs to identify the primary modes of morphological variation. For each group, the number of components required to account for 85% of the total variance was determined and used to compare variation patterns between asymptomatic and pathological SSMs.

Table 1
Morphological parameters used to characterise scapular shape.

ID	Name	Unit	Definition
GH	Glenoid height	mm	Distance between the inferior and superior glenoid borders, representing the vertical dimension of the glenoid surface.
GW	Glenoid width	mm	Distance between the posterior and anterior glenoid borders, representing the horizontal dimension of the glenoid.
GI_p	Morphological inclination	°	Angle between the superior-inferior glenoid axis and the line tangent to the scapular spine.
GI_m	Positional inclination	°	Angle between the superior-inferior glenoid axis and the vertical ground reference.
GV	Glenoid version	°	Angle between the line connecting the anterior and posterior glenoid margins and a line perpendicular to the scapular body in the axial plane.
CSA	Critical shoulder angle	°	Angle between the line connecting the superior and inferior glenoid borders and the line extending from the inferior glenoid border to the most lateral point of the acromion, measured in the anteroposterior plane.

2.3. Generation of scapulae using statistical shape models

A total of 1000 right scapulae were generated using the SSMs, with equal numbers drawn from the asymptomatic and pathological models to ensure balanced representation in the ARM estimation. This sample size was selected through a sensitivity analysis performed by re-estimating ARMs using sample sizes ranging from 10 to 5000 SSM-generated scapulae (available in Supplementary Material). The samples were generated using a uniform distribution within the shape space, bounded by ± 3 standard deviations derived from the square root of the corresponding PCA eigenvalues, to explore the morphological space broadly and without bias, and to avoid over-representation of mean shapes that would arise from a normal distribution given the limited representativeness of the available population. All models (participant models, SSMs, SSM-generated models) shared a consistent mesh topology, with identical vertex count and anatomical correspondence. Specifically, each anatomical landmark was always associated to the same vertex in the mesh.

2.4. Compared local coordinate systems

Eleven local coordinate systems (LCSs) were assessed this study. These LCSs, previously identified in the literature (Moissenet et al., 2025b), are assumed to be representative of current practices in

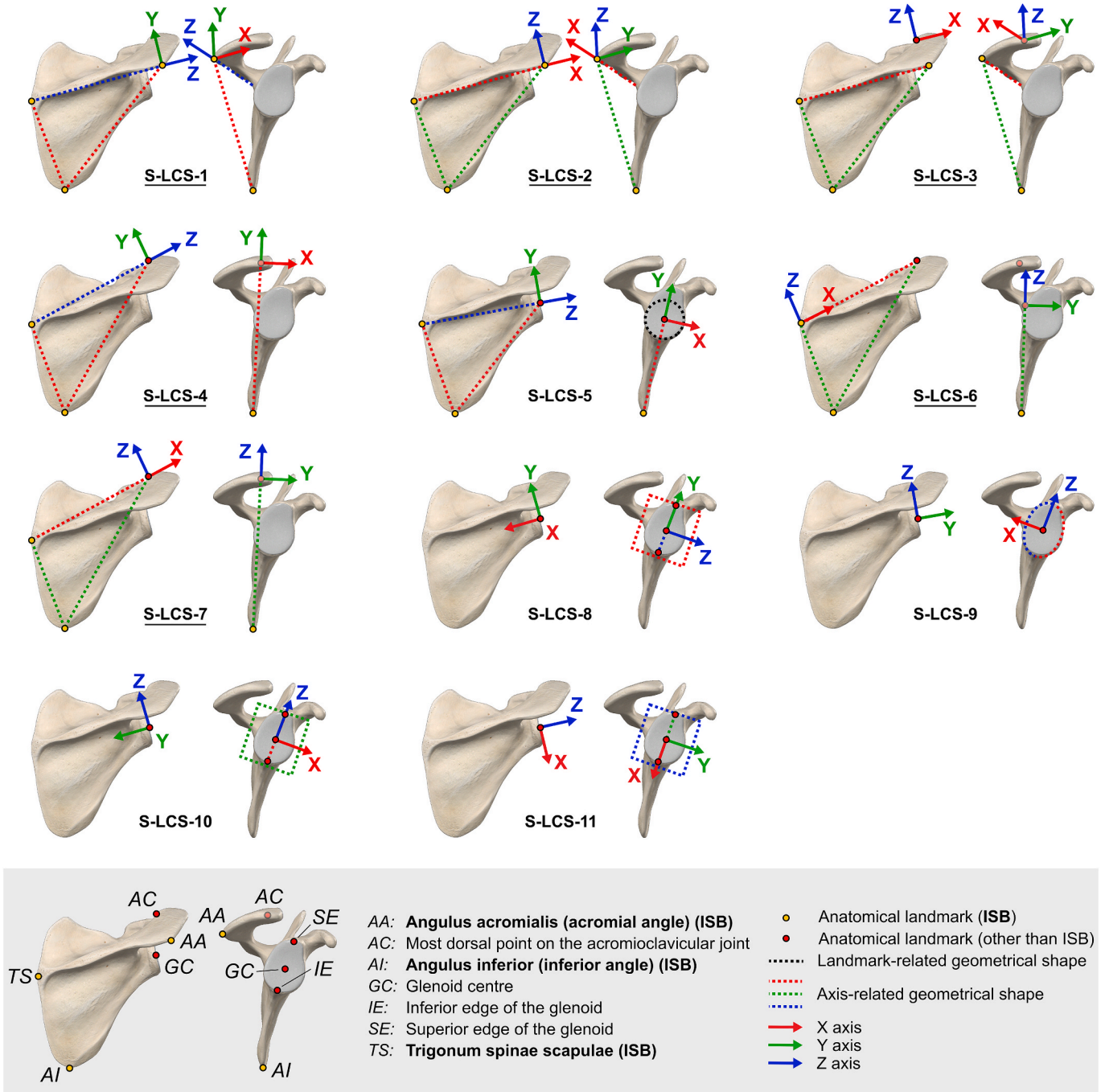

Fig. 1. Local coordinate systems (LCSs) of the scapula. S-LCS-1 stands for the LCS recommended by the International Society of Biomechanics (ISB) (Wu et al., 2005). S-LCS-2 to S-LCS-11 represent 10 alternative LCSs characterised by distinct anatomical landmarks and axis constructions. Scapula-based LCSs are indicated by underlined labels.

shoulder kinematic analysis (Fig. 1). The selection includes the ISB-recommended LCS (Wu et al., 2005) (S-SCS-1), alongside 10 alternative definitions characterised by distinct anatomical landmarks and axis constructions (S-SCS-2 to S-SCS-11). These LCSs can be categorised into six "scapula-based" LCSs (S-LCS-1–4,6–7), typically constructed from palpable landmarks (e.g., acromial angle, trigonum spinae, and inferior angle), and five "glenoid-based" LCSs (S-LCS-5,8–11), which rely on landmarks and geometric features accessible through medical imaging (e.g., glenoid centre, and glenoid best fit plane). In particular, S-LCS-4 and S-LCS-5 correspond to the acromioclavicular joint-centred LCS and glenoid-centred LCS defined by Kolz et al. (2020).

All LCSs were reconstructed on each SSM-generated scapula using anatomical landmarks, following the definitions detailed in Supplementary Table S1. Since each anatomical landmark was consistently associated with the same vertex across all meshes, the construction of LCSs remained consistent throughout all SSM-generated scapulae.

2.5. Computation of average rotation matrices

For each SSM-generated scapula, rotation matrices describing the transformation from each alternative LCS (S-LCS-2 to S-LCS-11) to the ISB-recommended LCS (S-LCS-1) were computed. To correct deviations in axes' orientations, an initial correction was applied to each alternative LCS $i \in \{2 \dots 11\}$ of each scapula $j \in \{1 \dots 1000\}$ using a rotation matrix ${}^{ISB_0}\mathbf{R}_i$ as follows:

$$\mathbf{R}_{i,j} = {}^{ISB_0}\mathbf{R}_i \mathbf{R}_{i,j}^{uncorrected} \quad (1)$$

This correction ensured that the LCS axes were approximately aligned with ISB-recommended anatomical directions (Wu et al., 2005): X was defined + posteroanterior (pointing anteriorly), Y was defined + inferosuperior (pointing superiorly), and Z was defined + mediolateral (pointing laterally). This correction only introduces ± 90° or ± 180° rotations around one or two axes.

To compute average rotation matrices $\overline{\mathbf{R}}_i$, the method proposed by Kolz et al. (2020) was used. First, for each alternative LCS i, the arithmetic mean of each element of the individual rotation matrices $\mathbf{R}_{i,j}$ across the 1000 SSM-generated scapulae was computed, resulting in a non-orthogonal matrix $\widetilde{\mathbf{R}}_i$. Second, to recover a proper rotation matrix, a singular value decomposition (SVD) was performed:

$$\widetilde{\mathbf{R}}_i = \mathbf{U}_i \Sigma_i \mathbf{V}_i^T \quad (2)$$

The final average (orthogonal) rotation matrix was obtained as:

$$\overline{\mathbf{R}}_i = \mathbf{U}_i \mathbf{V}_i^T \quad (3)$$

The overall transformation for each alternative LCS i of each scapula j can then be expressed as:

$$\mathbf{R}_i = \overline{\mathbf{R}}_i^{ISB_0} \mathbf{R}_i \quad (4)$$

This matrix $\mathbf{R}_i$ can be applied to the original uncorrected alternative LCS i of each scapula j to convert resulting in a compensated transformation into the ISB-recommended LCS:

$$\mathbf{R}_{i,j}^{corrected} = \mathbf{R}_i \mathbf{R}_{i,j}^{uncorrected} \quad (5)$$

2.6. Orientation errors

Before applying the average rotation matrix approach, the minimal angle of rotation θ_0 was computed, for each of the 1000 SSM-generated scapulae, between each pair of LCS. This analysis was based on the LCSs corrected for axes' orientation (${}^{ISB_0}\mathbf{R}_i$) but not yet adjusted using average rotations matrices ($\overline{\mathbf{R}}_i$), thereby quantifying the initial angular variability in the LCSs.

For all alternative LCS (S-LCS-2 to S-LCS-11), the minimal angle of rotation θ_a was computed, for each of the 1000 SSM-generated scapulae, between each scapula-specific rotation matrix (i.e., the rotation matrix describing the rigid transformation between the alternative LCS and the ISB-recommended LCS) and the corresponding average rotation matrix, thereby quantifying the accuracy of the average rotation matrix approach.

For S-LCS-4 and S-LCS-5, the minimal angle of rotation θ_k was computed, for each of the 1000 SSM-generated scapulae, between the LCS resulting from our average rotation matrix and the one reported by Kolz et al. (2020), thereby illustrating the influence of dataset- and population-specific factors on the average rotation matrix approach.

In all cases, the minimal angle of rotation θ between two LCSs $\mathbf{R}_1$ and $\mathbf{R}_2$ was computed with the helical angle as follows:

$$\theta = cos^{-1}\left(\frac{\mathrm{Tr}\left(\mathbf{R}_1^T \mathbf{R}_2\right) - 1}{2}\right) \quad (6)$$

3. Results

3.1. Dataset

The mean and standard deviation of morphological parameters (Table 1) for both the asymptomatic and symptomatic groups are reported in Table 2. Notably, the morphological inclination (GI_p) and the critical shoulder angle (CSA) demonstrated statistically significant differences between the two groups, while the morphological inclination (GI_p), the positional inclination (GI_m), and the glenoid version (GV) exhibited high variability across both groups, with retroverted glenoids

Table 2
Descriptive statistics of the six morphological parameters related to the scapulae included to the dataset for each group (A: asymptomatic group, P: pathological group): GH: Glenoid height; GW: Glenoid width; GI_p: Positional inclination angle of the glenoid; GI_m: Morphological inclination angle of the glenoid; GV: Glenoid version; CSA: Critical shoulder angle.

Parameters	Group	Mean	±	SD	[Min,	Max]	CV (%)	*t*-test
GH (mm)	A	34.7	±	3.8	[27.7,	41.4]	10.8	$p > 0.05$
	P	34.9	±	3.4	[27.1,	40.9]	9.8	
GW (mm)	A	25.6	±	3.0	[19.2,	30.8]	11.5	$p > 0.05$
	P	25.7	±	2.5	[20.4,	30.1]	9.7	
GIp (°)	A	6.0	±	6.8	[0.2,	30.3]	113.0	**$p = 0.03$**
	P	10.9	±	10.5	[0.0,	37.8]	95.7	
GIm (°)	A	1.8	±	2.9	[-4.0,	6.7]	160.0	$p > 0.05$
	P	1.2	±	3.6	[-9.7,	8.5]	295.0	
GV (°)	A	2.1	±	2.7	[-11.0,	4.4]	129.0	$p > 0.05$
	P	2.4	±	0.5	[1.2,	3.6]	20.9	
CSA (°)	A	34.1	±	3.6	[27.1,	41.7]	10.5	**$p = 0.007$**
	P	36.7	±	4.1	[28.0,	47.4]	11.3	

Notes: SD: Standard deviation; Min: Minimum; Max: Maximum; CV: Coefficient of variation; *t*-test: p-value calculated using Student's *t*-test between asymptomatic and symptomatic groups.

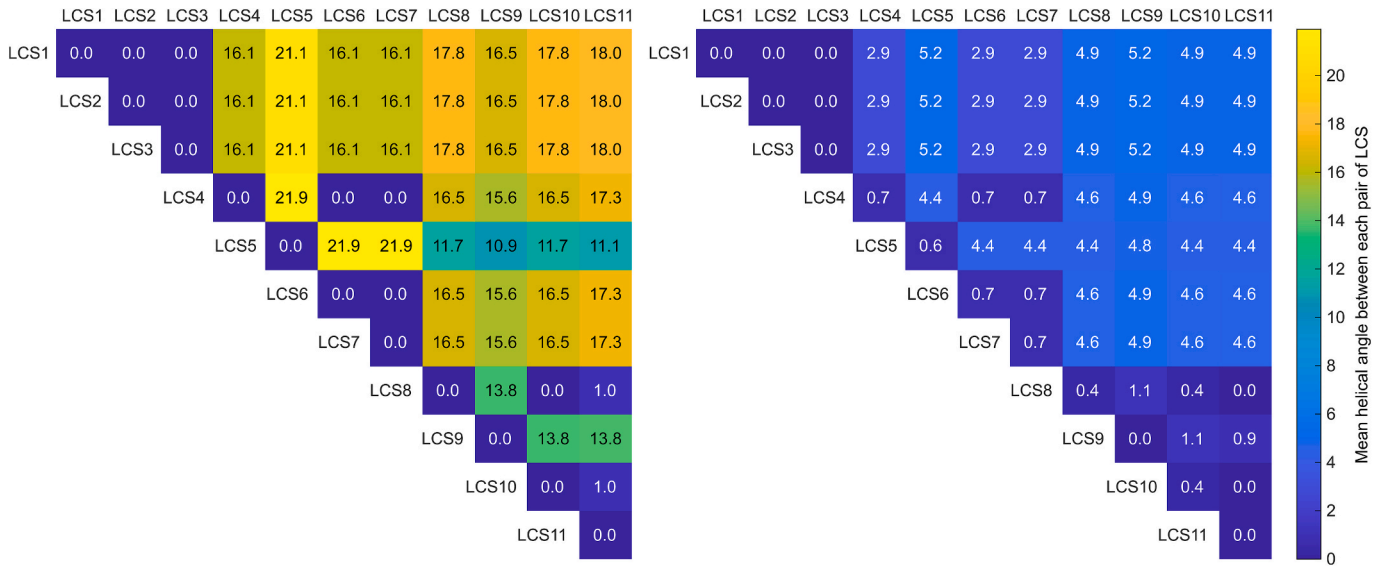

Fig. 2. Pairwise mean helical angle in degrees between local coordinate systems (LCSs, LCS1 being the ISB recommended-LCS), computed after correcting for axes orientation deviations $\left({}^{ISB_0}\mathbf{R}_i\right)$, but before (left) and after (right) applying the average rotation matrices.

observed exclusively in the asymptomatic group.

3.2. Statistical shape models

The PCA revealed distinct but overlapping patterns of morphological variation between the asymptomatic and pathological models. Seven principal components were required to exceed 85% of variance in the asymptomatic model, compared to eight in the pathological model. Both models showed changes in (a) the inferior angle (position/size in the asymptomatic model; orientation/size in the pathological model), (b) the acromion (position/size/shape in both groups), (c) the glenoid (shape/size in both groups), and (d) the coracoid process (position in both groups). Additionally, only the asymptomatic model involved variation in the orientation of the superior angle and in the position and size of the scapular spine.

3.3. Angular variability in the local coordinate systems

Overall, the mean helical angle between each pair of LCSs after correcting for axes orientation deviations but before applying the average rotation matrices θ_0 ranged 0.0° to 21.9° (Fig. 2). This difference decreased for all pairs of LCSs after applying the average rotation matrices (θ_a), ranging then from 0.0° to 5.2°.

3.4. Average rotation matrices

The average rotation matrices $\mathbf{R}_i$ describing the transformation from each LCS i to the ISB-recommended LCS (S-LCS-1) are reported below. These matrices define the rigid body transformations that align each alternative LCS with the ISB-recommended LCS (S-LCS-1) (matrices ${}^{ISB_0}\mathbf{R}_i$ and $\overline{\mathbf{R}}_i$ are available with 15-digit precision in Supplementary Tables S2 and S3):

$$\mathbf{R}_1 = \begin{bmatrix} 1 & 0 & 0 \\ 0 & 1 & 0 \\ 0 & 0 & 1 \end{bmatrix}$$
S-SCS-1

$$\mathbf{R}_2 = \begin{bmatrix} 0 & 0 & 1 \\ 1 & 0 & 0 \\ 0 & 1 & 0 \end{bmatrix}$$
S-SCS-2

$$\mathbf{R}_3 = \begin{bmatrix} 0 & 0 & 1 \\ 1 & 0 & 0 \\ 0 & 1 & 0 \end{bmatrix}$$
S-SCS-3

$$\mathbf{R}_4 = \begin{bmatrix} 0.9781 & -0.0002 & -0.2083 \\ -0.0376 & 0.9834 & -0.1775 \\ 0.2049 & 0.1814 & 0.9618 \end{bmatrix}$$
S-SCS-4

$$\mathbf{R}_5 = \begin{bmatrix} 0.9521 & -0.0025 & -0.3059 \\ 0.0580 & 0.9833 & 0.1726 \\ 0.3004 & -0.1821 & 0.9363 \end{bmatrix}$$
S-SCS-5

$$\mathbf{R}_6 = \begin{bmatrix} 0.2049 & 0.1814 & 0.9618 \\ 0.9781 & -0.0002 & -0.2083 \\ -0.0376 & 0.9834 & -0.1775 \end{bmatrix}$$
S-SCS-6

$$\mathbf{R}_7 = \begin{bmatrix} 0.2049 & 0.1814 & 0.9618 \\ 0.9781 & -0.0002 & -0.2083 \\ -0.0376 & 0.9834 & -0.1775 \end{bmatrix}$$
S-SCS-7

$$\mathbf{R}_8 = \begin{bmatrix} -0.2500 & 0.0560 & -0.9666 \\ 0.1494 & 0.9886 & 0.0186 \\ 0.9566 & -0.1398 & -0.2556 \end{bmatrix}$$
S-SCS-8

$$\mathbf{R}_9 = \begin{bmatrix} -0.9648 & -0.0991 & 0.2436 \\ 0.2499 & -0.0560 & 0.9667 \\ -0.0821 & 0.9935 & 0.0788 \end{bmatrix}$$
S-SCS-9

$$\mathbf{R}_{10} = \begin{bmatrix} 0.9566 & -0.1398 & -0.2556 \\ -0.2500 & 0.0560 & -0.9666 \\ 0.1494 & 0.9886 & 0.0186 \end{bmatrix}$$
S-SCS-10

$$\mathbf{R}_{11} = \begin{bmatrix} -0.1536 & -0.9875 & -0.0350 \\ 0.9566 & -0.1398 & -0.2556 \\ 0.2475 & -0.0727 & 0.9662 \end{bmatrix}$$
S-SCS-11

3.5. Accuracy of the average rotation matrix approach

Overall, the mean helical angle θ_a between each model-specific rotation matrix and the related average rotation matrix was higher, and more widely distributed, for all glenoid-based LCSs compared to scapula-based LCSs. Nevertheless, for each alternative scapula-based LCS (S-LCS-2 to S-LCS-11), θ remained within a range of up to 5.2 ± 2.7° (Fig. 3).

To assess the robustness of the approach with respect to dataset- and population-specific factors, the average rotation matrices obtained in the present study were compared with those reported by Kolz et al. (2020). The mean helical angle θ_k between the resulting LCSs was 2.8° for S-LCS-4 and 2.2° for S-LCS-5.

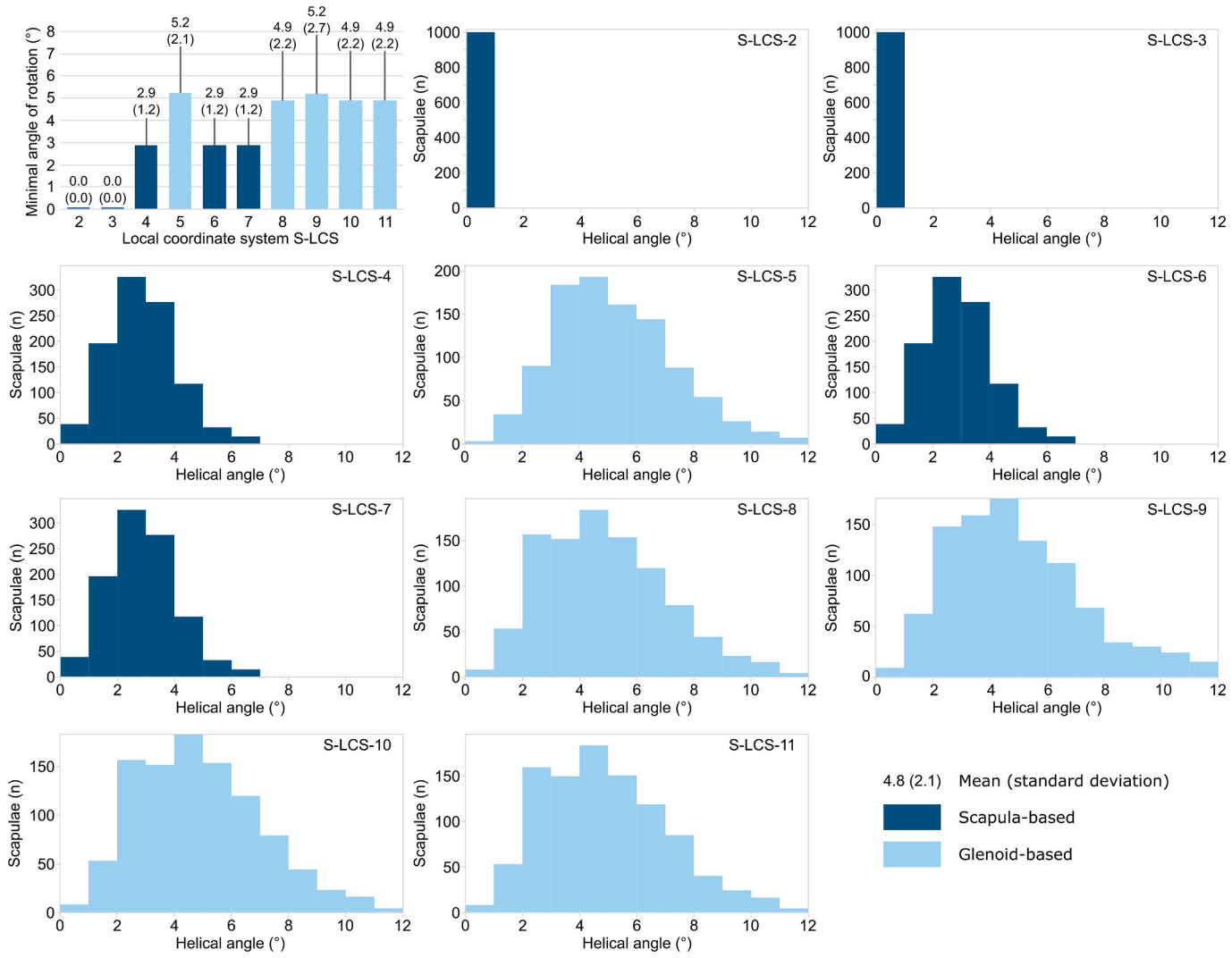

Fig. 3. Mean (standard deviation) and error distribution histograms of the helical angle (°) between model-specific and average rotation matrices aligning each alternative local coordinate system (LCS) with the ISB-recommended LCS.

4. Discussion

This study aimed to assess the compatibility of 11 scapular LCSs by quantifying the helical angle between each system and the ISB-recommended LCS across 1000 statistically generated scapulae. Building on the process proposed by Kolz et al. (2020), we have tested the generalisability of average rotation matrices to a broader range of LCSs, comprising both scapula- and glenoid-based LCSs, and evaluated whether the results hold across a larger and more morphologically variable dataset. Importantly, we have not treated differences between LCSs as measurement errors to be corrected, as would be appropriate for crosstalk reduction in the knee (e.g., using the reference frame alignment method proposed by Ortigas Vásquez et al. (2023)), but rather as equally plausible alternatives reflecting different anatomical conventions. Overall, the application of average rotation matrices reduced the mean helical angle between scapular LCSs from values of up to 21.2° to less than 5.2° across all tested systems, thereby substantially improving comparability between coordinate system definitions.

4.1. Generalisation of the approach to eleven local coordinate systems

Our results confirmed that average rotation matrices remain valid across all tested LCSs, with low mean helical angle across all tested LCSs. This supports our first hypothesis that the approach remains valid even when extended to a wider range of LCSs than the ones used by Kolz et al. (2020). Importantly, this approach reduced the discrepancies observed between LCSs from values as high as 21.2° (after correcting for axes orientation deviations ${}^{ISB_0}\mathbf{R}_i$) down to less than 5.2°, thereby substantially improving the consistency of coordinate system conversions. This robustness is especially relevant in biomechanics research and clinical practice, where data interoperability between laboratories or studies using different LCSs is a known challenge (Kolz et al., 2020; Lawrence et al., 2022; Moissenet et al., 2025b). The relatively small angular deviations observed in these conversions provide confidence for the use of large scapular datasets, including retrospective analyses.

4.2. Impact of glenoid-based definitions and morphological variation

While the average rotation matrix approach was applicable across all LCSs, glenoid-based LCSs led to higher rotational discrepancies. These results support our second hypothesis and are in line with the morphological findings presented in Table 1. Indeed, the glenoid region exhibited greater shape variability, particularly in parameters such as the glenoid version (GV) and the morphological inclination (GIp), which directly influence the orientation of glenoid-based axes. The comparison of morphological parameters between asymptomatic and pathological groups indicated that the dataset encompassed a broad spectrum of scapular morphologies. This variability strengthens the relevance of the

average rotation matrix approach, as it was evaluated across a wide range of anatomical configurations. The inclusion of both asymptomatic and pathological scapulae was intended to maximise morphological variability, representative of the general population (Elshahhat et al., 2025; Gumina et al., 2022). Despite statistical group differences, parameter distributions largely overlapped, indicating that residual ARM errors reflect combined anatomical variability and LCS definition rather than pathology-specific deformation.

As a result, our average rotation matrices are more affected by local anatomical differences in these LCSs. Interestingly, despite this increased variability, the angular differences for the glenoid-based LCSs remained within a reasonable range, with a maximum mean helical angle of 5.2° (where scapula-based LCSs were up to 2.9°). This suggests that while glenoid-based systems may be more sensitive to inter-individual anatomical variation, the use of average rotation matrices remains an acceptable solution for harmonising kinematic data.

4.3. Comparison with previously published matrices

In addition to assessing the performance of the average rotation matrix approach across all LCSs, we compared our results with those reported by Kolz et al. (2020). Despite differences in datasets, sample size, and processing pipelines, the average rotation matrices derived in our study for S-LCS-4 (acromioclavicular-based) and S-LCS-5 (glenoid-based) showed minimal rotational discrepancies (2.8° and 2.2°, respectively) when compared with those from Kolz et al. (2020). This finding supports our third hypothesis and reinforces the generalisability of the approach across populations. Moreover, these results demonstrate that while the absolute orientation of average frames may differ slightly due to sample characteristics, the relative transformations remain robust. This highlights the potential of average rotation matrices not only for inter-study alignment, but also for enabling the pooling of datasets constructed using different coordinate systems.

4.4. Limitations and future work

Several limitations must be acknowledged. First, our approach relied on average rotation matrices. A natural next step would be to develop subject-specific conversion matrices, for instance as a function of easily measurable morphological parameters such as the distance between the trigonum spinae and the acromioclavicular joint. Second, although the use of SSM-generated scapulae offers statistical generalisability, it does not fully capture the inter- and intraoperator variability in landmark placement (Moissenet et al., 2025a) or segmentation uncertainty (Schnider et al., 2022) that may affect real-world applications. Third, our analysis focused exclusively on geometric transformations and did not consider functional implications, such as the impact of LCS choice on joint angle computation during dynamic tasks. Future studies may investigate dynamic datasets and motion trials to assess the propagation of these rotational discrepancies into joint kinematics. Fourth, the threshold for acceptable rotational discrepancy remains somewhat arbitrary and should be interpreted with application-specific context. Importantly, error quantification alone does not constitute validation. It only characterises uncertainty under the tested conditions. Future studies may provide formal validation by demonstrating, against imaging-based or experimental ground truth, that conversions between LCSs preserve posture- and task-level conclusions across independent cohorts, dynamic tasks, and analysis pipelines. Finally, severe glenoid deformities (e.g., Walch B-type), which were not represented in our dataset, may limit the applicability of the proposed average rotation matrices. Assessing the validity of ARM-based transformations in the presence of substantial glenoid remodelling remains a relevant direction for future work.

4.5. Conclusion

This study confirms the applicability of average rotation matrices as a robust postprocessing solution to quantify and compensate for rotational discrepancies between scapular local coordinate systems (LCSs). By extending this method to 11 LCSs and validating its performance across a large and morphologically diverse dataset, we provide evidence supporting its generalisation beyond the original scope of Kolz et al. (2020). Our findings highlight the value of average rotation matrices for enhancing data interoperability and reproducibility in shoulder biomechanics research.

5. Code and data availability

The average rotation matrices computed in this study are available in Supplementary Tables S2 and S3.

CRediT authorship contribution statement

Florent Moissenet: Writing – review & editing, Writing – original draft, Visualization, Validation, Supervision, Resources, Methodology, Investigation, Formal analysis, Data curation, Conceptualization. **Benjamin Michaud:** Writing – review & editing, Validation, Software, Methodology, Data curation. **Pierre Puchaud:** Writing – review & editing, Validation, Software, Methodology, Data curation. **Nicola Hagemeister:** Writing – review & editing, Writing – original draft, Funding acquisition. **Mickaël Begon:** Writing – review & editing, Writing – original draft, Resources, Methodology, Funding acquisition, Conceptualization. **Nicolas Holzer:** Writing – review & editing, Funding acquisition, Conceptualization.

Declaration of competing interest

The authors declare that they have no known competing financial interests or personal relationships that could have appeared to influence the work reported in this paper.

Acknowledgments

We gratefully acknowledge Dr. Heath Henninger for his insightful discussions on the calculation and application of transformation matrices.

Appendix A. Supplementary data

Supplementary data to this article can be found online at https://doi.org/10.1016/j.jbiomech.2026.113219.

References

Bascan, C., 2018. Évaluation morpho-fonctionnelle de l'épaule (Mémoire de maîtrise en génie des technologies de la santé). Université du Québec, Montréal.

Casier, S.J., Van den Broecke, R., Van Houcke, J., Audenaert, E., De Wilde, L.F., Van Tongel, A., 2018. Morphologic variations of the scapula in 3-dimensions: a statistical shape model approach. J. Shoulder Elbow Surg. 27, 2224–2231. https://doi.org/10.1016/j.jse.2018.06.001.

Churchill, R.S., Brems, J.J., Kotschi, H., 2001. Glenoid size, inclination, and version: an anatomic study. J. Shoulder Elbow Surg. 10, 327–332. https://doi.org/10.1067/mse.2001.115269.

Cresson, T., Godbout, B., Branchaud, D., Chav, R., Gravel, P., De Guise, J.A., 2008. Surface reconstruction from planar x-ray images using moving least squares. In: 2008 30th Annual International Conference of the IEEE Engineering in Medicine and Biology Society. Presented at the 2008 30th Annual International Conference of the IEEE Engineering in Medicine and Biology Society, pp. 3967–3970. https://doi.org/10.1109/IEMBS.2008.4650078.

Dumas, R., Chèze, L., Verriest, J.-P., 2007. Adjustments to McConville et al. and Young et al. body segment inertial parameters. Journal of Biomechanics 40, 543–553. DOI: 10.1016/j.jbiomech.2006.02.013.

Elshahhat, A., Basyoni, Y., Nour, K., 2025. Comprehensive analysis of bony scapula morphology and anthropometry in a homogeneous population. BMC Med. Imaging 25, 262. https://doi.org/10.1186/s12880-025-01793-z.

Goutallier, D., Postel, J.M., Bernageau, J., Lavau, L., Voisin, M.C., 1994. Fatty muscle degeneration in cuff ruptures. pre- and postoperative evaluation by CT scan. Clin. Orthop. Relat. Res. 78–83.

Gumina, S., Polizzotti, G., Spagnoli, A., Carbone, S., Candela, V., 2022. Critical shoulder angle (CSA): age and gender distribution in the general population. J. Orthop. Traumatol. 23, 10. https://doi.org/10.1186/s10195-022-00627-w.

Hagemeister, N., Lagacé, P.-Y., Gregori, J.H., Marck, L., Rouleau, D., Bureau, N.J., Tétreault, P., Roy, A., Al-Shakfa, F., 2014. Développement d'un indice radiologique représentatif de la fonction de l'épaule chez des travailleurs souffrant de rupture de la coiffe des rotateurs (Rapports de recherche scientifique No. R-812), IRSST. École de technologie supérieure, Montréal.

İncesoy, M.A., Yıldız, K.İ., Türk, Ö.İ., Akıncı, Ş., Turgut, E., Aycan, O.E., Bayhan, I.A., 2021. The critical shoulder angle, the acromial index, the glenoid version angle and the acromial angulation are associated with rotator cuff tears. Knee Surg. Sports Traumatol. Arthrosc. 29, 1795. https://doi.org/10.1007/s00167-020-06145-8.

Kolz, C.W., Sulkar, H.J., Aliaj, K., Tashjian, R.Z., Chalmers, P.N., Qiu, Y., Zhang, Y., Foreman, K.B., Anderson, A.E., Henninger, H.B., 2020. Reliable interpretation of scapular kinematics depends on coordinate system definition. Gait Posture 81, 183–190. https://doi.org/10.1016/j.gaitpost.2020.07.020.

Lawrence, R.L., Roseni, K., Bey, M.J., 2022. Correspondence between scapular anatomical coordinate systems and the 3D axis of motion: a new perspective on an old challenge. J. Biomech. 145, 111385. https://doi.org/10.1016/j.jbiomech.2022.111385.

Moissenet, F., Boudabbous, S., Holzer, N., 2025a. Impact of scapula anatomical landmark positioning on scapular orientation using CT-based 3-dimensional models: an intraobserver repeatability and interobserver reproducibility study. JSES International 9, 524–531. https://doi.org/10.1016/j.jseint.2024.09.027.

Moissenet, F., Puchaud, P., Naaim, A., Holzer, N., Begon, M., 2025b. Spartacus: a review and aggregation of reference datasets reporting the normal shoulder girdle kinematics during uniplanar humerus motions. J. Biomech. 189, 112642. https://doi.org/10.1016/j.jbiomech.2025.112642.

Moor, B.K., Bouaicha, S., Rothenfluh, D.A., Sukthankar, A., Gerber, C., 2013. Is there an association between the individual anatomy of the scapula and the development of rotator cuff tears or osteoarthritis of the glenohumeral joint? The Bone & Joint Journal 95-B, 935–941. https://doi.org/10.1302/0301-620X.95B7.31028.

Ohl, X., Billuart, F., Lagacé, P.-Y., Gagey, O., Hagemeister, N., Skalli, W., 2012. 3D morphometric analysis of 43 scapulae. Surg. Radiol. Anat. 34, 447–453. https://doi.org/10.1007/s00276-012-0933-z.

Ortigas Vásquez, A., Taylor, W.R., Maas, A., Woiczinski, M., Grupp, T.M., Sauer, A., 2023. A frame orientation optimisation method for consistent interpretation of kinematic signals. Sci. Rep. 13, 9632. https://doi.org/10.1038/s41598-023-36625-z.

Satir, O.B., Eghbali, P., Becce, F., Goetti, P., Meylan, A., Rothenbühler, K., Diot, R., Terrier, A., Büchler, P., 2024. Automatic quantification of scapular and glenoid morphology from CT scans using deep learning. Eur. J. Radiol. 177. https://doi.org/10.1016/j.ejrad.2024.111588.

Schnider, E., Huck, A., Toranelli, M., Rauter, G., Zam, A., Müller-Gerbl, M., Cattin, P., 2022. Ensemble uncertainty as a criterion for dataset expansion in distinct bone segmentation from upper-body CT images.

Smith, G.C.S., Geelan-Small, P., Sawang, M., 2022. A predictive model for the critical shoulder angle based on a three-dimensional analysis of scapular angular and linear morphometrics. BMC Musculoskelet. Disord. 23, 1006. https://doi.org/10.1186/s12891-022-05920-7.

Sulkar, H.J., Zitnay, J.L., Aliaj, K., Henninger, H.B., 2021. Proximal humeral coordinate systems can predict humerothoracic and glenohumeral kinematics of a full bone system. Gait Posture 90, 380–387. https://doi.org/10.1016/j.gaitpost.2021.09.180.

Thomazeau, H., Rolland, Y., Lucas, C., Duval, J.M., Langlais, F., 1996. Atrophy of the supraspinatus belly. assessment by MRI in 55 patients with rotator cuff pathology. Acta Orthop. Scand. 67, 264–268. https://doi.org/10.3109/17453679608994685.

Tokita, R., Toda, H., Imamura, R., Sugi, A., Shibayama, Y., 2025. Scapular morphological variations and sex-related and generational differences in global scapular shape: three-dimensional morphometric analysis using a homologous model. JSES Reviews, Reports & Techniques. https://doi.org/10.1016/j.xrrt.2025.04.001.

Umeyama, S., 1991. Least-squares estimation of transformation parameters between two point patterns. IEEE Trans. Pattern Anal. Mach. Intell. 13, 376–380. https://doi.org/10.1109/34.88573.

Wu, G., van der Helm, F.C.T., (DirkJan) Veeger, H.E.J., Makhsous, M., Van Roy, P., Anglin, C., Nagels, J., Karduna, A.R., McQuade, K., Wang, X., Werner, F.W., Buchholz, B., 2005. ISB recommendation on definitions of joint coordinate systems of various joints for the reporting of human joint motion—Part II: shoulder, elbow, wrist and hand. Journal of Biomechanics 38, 981–992. DOI: 10.1016/j.jbiomech.2004.05.042.

Xu, X., Lin, J.-H., Li, K., Tan, V., 2012. Transformation between different local coordinate systems of the scapula. J. Biomech. 45, 2724–2727. https://doi.org/10.1016/j.jbiomech.2012.08.021.

Yamani, L., 2022. Étude morphologique des structures osseuses de l'épaule par la caractérisation d'un modèle statistique (Mémoire de maîtrise en génie des technologies de la santé). Université du Québec, Montréal.

Zhang, C., 2016. Contribution à la modélisation morphofonctionnelle 3D de l'épaule (Thèse de doctorat en cotutelle). École de technologie supérieure (Université du Québec) et Arts et Métiers ParisTech, Montréal.

Zhou, J., Zhong, B., Qu, R., Qian, L., Li, Z., Liu, C., Xiao, Z., Xu, G., Liang, H., Wei, K., Ouyang, J., Dai, J., 2022. Anatomic measurement of osseous parameters of the glenoid. Sci. Rep. 12, 13424. https://doi.org/10.1038/s41598-022-17783-y.